International Journal of Applied Mathematics

Volume 38 No. 11s, 2025

ISSN: 1311-1728 (printed version); ISSN: 1314-8060 (on-line version

A VARIATIONAL RAYLEIGH–RITZ SOLUTION FOR NONLINEAR MULTIPHASE MAGNETOHYDRODYNAMIC NANOFLUID FLOW AND HEAT TRANSFER OVER A PERMEABLE STRETCHING/SHRINKING SURFACE EMBEDDED IN A POROUS MEDIUM

Tejas B shah[1], Kaushal B Patel[2],

[1]Department of Mathematics, Veer Narmad South Gujarat University, Surat.

[2]Narmada College of Science and Commerce, Bharuch.

Abstract

This study presents a variational Rayleigh–Ritz solution for nonlinear magnetohydrodynamic (MHD) multiphase nanofluid flow and heat transfer over a permeable stretching/shrinking surface embedded in a porous medium. The mathematical model incorporates the combined effects of porous medium permeability, thermal radiation, wall transpiration, and higher-order Navier slip conditions. Blood-based nanofluids containing Silver (Ag) and Copper (Cu) nanoparticles are considered to investigate the influence of nanoparticle-enhanced thermophysical properties on momentum and thermal transport. The governing partial differential equations are transformed into coupled nonlinear ordinary differential equations using similarity transformations. A modified constrained Rayleigh–Ritz variational formulation is developed by constructing suitable exponential trial functions for the momentum and temperature fields. The higher-order slip and thermal boundary conditions are incorporated through constraint elimination, and exact analytical integration of the variational functionals yields nonlinear algebraic systems for the unknown Ritz coefficients. The resulting semi-analytical solutions are used to examine the effects of the magnetic parameter, porous medium permeability, nanoparticle volume fraction, wall transpiration, slip parameters, and thermal radiation on the velocity and temperature distributions. The results demonstrate that the magnetic field suppresses the fluid velocity while enhancing the thermal boundary layer, whereas higher-order slip significantly modifies the flow and heat transfer characteristics. The proposed constrained Rayleigh–Ritz method provides an accurate and computationally efficient semi-analytical framework for solving coupled nonlinear multiphase fluid flow problems in porous media and offers an effective alternative to conventional numerical methods.

Keywords: Rayleigh–Ritz method; Multiphase nanofluid; Magnetohydrodynamics; Porous medium; Blood-based nanofluid; Higher-order Navier slip; Thermal radiation.

1. Introduction

Magnetohydrodynamic (MHD) nanofluid flow has attracted considerable research interest because of its applications in thermal engineering, biomedical systems, electronic cooling, and energy conversion technologies [6–8,12]. Nanofluids, introduced by Choi et al. [3], are engineered suspensions of nanoparticles in conventional base fluids that exhibit enhanced

Received: Aug 12 2025

thermal conductivity and improved heat transfer characteristics. These superior thermophysical properties have made nanofluids promising candidates for advanced cooling technologies and biomedical transport applications [3,12].

The interaction of electrically conducting nanofluids with external magnetic fields generates Lorentz forces that provide effective control over fluid motion and thermal transport, making MHD nanofluid models suitable for applications such as magnetic drug delivery, cancer hyperthermia, and microscale flow regulation [7,8]. Furthermore, higher-order Navier slip boundary conditions become essential for accurately describing fluid behavior near solid surfaces in micro- and nanoscale transport systems [4,7]. The presence of porous media, commonly modelled using the Brinkman formulation [2], and thermal radiation, represented through the Rosseland approximation [11], further complicate the governing transport equations.

The coupled effects of magnetic fields, porous media, slip conditions, and thermal radiation produce highly nonlinear boundary value problems that generally require efficient analytical or semi-analytical solution techniques. In the present work, a modified constrained variational Rayleigh–Ritz method is developed to obtain semi-analytical solutions for nonlinear multiphase MHD nanofluid flow and heat transfer over a permeable stretching/shrinking surface embedded in a porous medium. The proposed approach transforms the governing equations into variational functionals and determines the unknown Ritz coefficients through constrained minimization, providing an accurate and computationally efficient alternative for nonlinear multiphase fluid flow problems.

2. Literature Review

The development of nanofluid technology by Choi et al. [3] initiated extensive research on enhanced heat transfer in nanoparticle suspensions. Tiwari and Das [12] demonstrated that nanoparticle volume fraction significantly improves thermal transport characteristics, establishing an important framework for subsequent nanofluid investigations. More recently, Maranna et al. [7] investigated non-Newtonian MHD nanofluid flow over a porous medium with Navier slip conditions and reported that magnetic field strength and slip parameters strongly influence the velocity and temperature distributions.

Further studies have incorporated thermal radiation, viscous dissipation, and nonlinear slip effects into MHD nanofluid models. Khan et al. [4] analyzed nonlinear thermal stratification and higher-order slip effects on radiated nanofluid flow through porous media, while Mane et al. [6] examined thermal radiation and variable-viscosity effects on MHD nanofluid flow over an exponentially stretching sheet. These studies demonstrated that magnetic fields generally suppress fluid motion, whereas thermal radiation significantly enhances thermal boundary layer development. The porous medium resistance in such models is commonly represented using the Brinkman equation [2], and radiative heat transfer is incorporated through the Rosseland diffusion approximation [11].

Similarity transformations are widely employed to reduce the governing partial differential equations into coupled nonlinear ordinary differential equations before solution. Various

International Journal of Applied Mathematics

Volume 38 No. 11s, 2025

ISSN: 1311-1728 (printed version); ISSN: 1314-8060 (on-line version

analytical, semi-analytical, and numerical approaches have been applied to these nonlinear boundary value problems, including Laplace transform methods [5], differential transformation methods [1,9,13,14], and numerical algorithms [10]. Although differential transformation methods provide accurate semi-analytical solutions for many nonlinear problems [1,13,14], most existing approaches rely on recursive formulations or numerical discretization.

In contrast, the Rayleigh–Ritz variational method transforms the nonlinear boundary value problem into an optimization problem by minimizing suitably constructed variational functionals. Despite its extensive application in classical boundary value problems, its use in nonlinear MHD multiphase nanofluid flow with higher-order slip, porous medium effects, and thermal radiation remains limited. The present work addresses this gap by developing a modified constrained variational Rayleigh–Ritz formulation, in which the boundary conditions are incorporated directly into the variational functional to obtain accurate semi-analytical solutions for the coupled momentum and thermal transport equations.

3. Problem Formulation and Mathematical Methods

Consider two-dimensional laminar flow of incompressible viscous nanofluid across a porous stretching/shrinking surface. The coordinate system has the x-axis along the stretching surface and the y-axis perpendicular to it. A uniform magnetic field B_0 is applied perpendicular to the fluid motion in the region $y > 0$. The surface stretches/shrinks with velocity proportional to distance from the origin, with surface temperature maintained at T_w and ambient temperature at T_∞.

The flow is governed by conservation principles:

Continuity Equation:

$$\frac{\partial u}{\partial x} + \frac{\partial v}{\partial y} = 0 \tag{1}$$

Momentum Equation:

$$u\frac{\partial u}{\partial x} + v\frac{\partial u}{\partial y} = -\frac{1}{\rho_f}\frac{\partial p}{\partial x} + \frac{\mu_{nf}}{\rho_{nf}}\frac{\partial^2 u}{\partial y^2} - \frac{\mu_{nf}}{\rho_{nf}K}u - \frac{\sigma_{nf}B_0^2}{\rho_{nf}}u \tag{2}$$

Energy Equation with Thermal Radiation:

$$u\frac{\partial T}{\partial x} + v\frac{\partial T}{\partial y} = \chi\frac{\partial^2 T}{\partial y^2} - \frac{1}{(\rho C_p)_{nf}}\frac{\partial q_r}{\partial y} \tag{3}$$

where u, v are velocity components in x and y directions; μ_{nf}, ρ_{nf} are dynamic viscosity and density of nanofluid; K is permeability; $\sigma_n f$ is electrical conductivity; χ is thermal diffusivity; q_r is radiative heat flux.

Velocity Boundary Conditions (Navier's first and second-order slip):

$$u(x,0) = d\alpha x + \lambda_1\left(\frac{\partial u}{\partial y}\right)_{y=0} + \lambda_2\left(\frac{\partial^2 u}{\partial y^2}\right)_{y=0}, \quad v = V_c, \quad u(x,\infty) \to 0 \tag{4}$$

Temperature Boundary Conditions (with thermal jump):

International Journal of Applied Mathematics

Volume 38 No. 11s, 2025

ISSN: 1311-1728 (printed version); ISSN: 1314-8060 (on-line version

$$T(x,0) = T_w, \quad T - T_\infty = \xi \left(\frac{\partial T}{\partial y}\right)_{y=0}, \quad T(x,\infty) = T_\infty \tag{5}$$

where d is stretching/shrinking parameter; λ_1 and λ_2 are first and second-order slip coefficients; V_c is mass transpiration factor; ξ is temperature jump parameter.

To reduce PDEs to ODEs, we employ similarity variables:

$$\eta = \sqrt{\frac{\alpha}{\nu_f}}y, \quad f(\eta) \text{ such that } u = \alpha x \frac{\partial f}{\partial \eta}, \quad v = -\sqrt{\alpha \nu_f} f(\eta)$$

$$\theta(\eta) = \frac{T - T_\infty}{T_w - T_\infty} \tag{6}$$

The transformed equations become

Momentum ODE:

$$\Gamma_1 \frac{\partial^3 f}{\partial \eta^3} + \Gamma_2 \left[f(\eta)\frac{\partial^2 f}{\partial \eta^2} - \left(\frac{\partial f}{\partial \eta}\right)^2\right] - (K_1\Gamma_1 + M)\frac{\partial f}{\partial \eta} = 0 \tag{7}$$

Energy ODE (with Rosseland approximation):

$$\Gamma_3(1 + N_r)\frac{\partial^2 \theta}{\partial \eta^2} + \mathrm{Pr}\Gamma_4 f(\eta)\frac{\partial \theta}{\partial \eta} = 0 \tag{8}$$

Transformed boundary conditions:

$$f(0) = V_c, \quad \left(\frac{\partial f}{\partial \eta}\right)_{\eta=0} = d + \lambda_1\left(\frac{\partial^2 f}{\partial \eta^2}\right)_{\eta=0} + \lambda_2\left(\frac{\partial^3 f}{\partial \eta^3}\right)_{\eta=0} \tag{9}$$

$$\theta(0) = 1 + \xi\frac{\partial \theta}{\partial \eta}|_0, \quad \left(\frac{\partial f}{\partial \eta}\right)_{\eta \to \infty} \to 0, \quad \theta(\eta \to \infty) \to 0 \tag{10}$$

Where, $K_1 = \frac{\mu_f}{\rho_f \alpha K}$ (permeability), $M = \frac{\sigma_{nf} B_0^2}{\rho_f \alpha}$ (Hartmann number), $P_r = \frac{\mu_f C_{p,f}}{k_f}$ (Prandtl number),

$N_r = \frac{16\sigma^* T_\infty^3}{3k^* k_f}$ (Radiation parameter), $\tilde{\lambda}_1 = \lambda_1\sqrt{\frac{\alpha}{\nu_f}}$ (Dimensionless 1st-order slip), $\tilde{\lambda}_2 = \lambda_2 \frac{\alpha}{\nu_f}$ (Dimensionless 2nd-order slip)

The effective properties are calculated using

$$\mu_{nf} = \frac{\mu_f}{(1-\phi)^{2.5}}$$

$$\rho_{nf} = \left[(1-\phi) + \phi\frac{\rho_s}{\rho_f}\right]\rho_f$$

$$\kappa_{nf} = \kappa_f \frac{\kappa_s + 2\kappa_f - 2\phi(\kappa_f - \kappa_s)}{\kappa_s + 2\kappa_f + \phi(\kappa_f - \kappa_s)}$$

$$(\rho C_p)_{nf} = (1-\phi)(\rho C_p)_f + \phi(\rho C_p)_s$$

Received: Aug 12 2025

International Journal of Applied Mathematics

Volume 38 No. 11s, 2025

ISSN: 1311-1728 (printed version); ISSN: 1314-8060 (on-line version

The dimensionless coefficients are

$$\Gamma_1 = \frac{\mu_{nf}}{\mu_f}, \quad \Gamma_2 = \frac{\rho_{nf}}{\rho_f}, \quad \Gamma_3 = \frac{\kappa_{nf}}{\kappa_f}, \quad \Gamma_4 = \frac{(\rho C_p)_{nf}}{(\rho C_p)_f}$$

Table 1: Base Fluid and Nanoparticle Properties

Material	Density (kg/m^3)	Thermal Conductivity (W/mK)	Specific Heat (J/kgK)
Blood	1033	0.492	3594
Silver	10500	429	235
Copper	8933	401	385

Numerical Methodology

The transformed nonlinear boundary layer equations governing the velocity and temperature fields, given by Eqs. (7) - (10), are solved approximately using the Rayleigh–Ritz variational method. The method converts the higher-order boundary value problem into a system of algebraic equations by minimizing suitable energy functionals.

Rayleigh–Ritz Formulation

Consider the momentum equation

$$\Gamma_1 f''' + \Gamma_2(ff'' - (f')^2) - (K_1\Gamma_1 + M)f' = 0 \tag{11}$$

subject to the boundary conditions

$$f(0) = V_c, \qquad f'(0) = d + \lambda_1 f''(0) + \lambda_2 f'''(0), \quad f'(\eta \to \infty) \to 0. \tag{12}$$

The above equation is associated with the functional

$$J_f = \int_0^\infty \left[\frac{\Gamma_1}{2}(f'')^2 - \frac{\Gamma_2}{2} f (f')^2 + \frac{(K_1\Gamma_1 + M)}{2}(f')^2\right] d\eta \tag{13}$$

whose stationary condition yields the governing momentum equation.

Similarly, the energy equation

$$\Gamma_3(1 + Nr)\theta'' + Pr\,\Gamma_4 f\theta' = 0 \tag{14}$$

Similarly, the thermal slip boundary condition

$$\theta(0) = 1 + \xi\theta'(0) \tag{15}$$

is represented by the functional

$$J_\theta = \int_0^\infty \left[\frac{\Gamma_3(1 + Nr)}{2}(\theta')^2 + \frac{Pr\,\Gamma_4}{2} f\theta^2\right] d\eta. \tag{16}$$

International Journal of Applied Mathematics

Volume 38 No. 11s, 2025

ISSN: 1311-1728 (printed version); ISSN: 1314-8060 (on-line version

Solution for momentum equation

Choose trail function as

$$f(\eta) = V_c + a_1(1 - e^{-\eta}) + a_2(1 - e^{-\eta})^2 \tag{17}$$

where a_1, a_2,are unknown constants to be determined.

$$f = A_0 - A_1 e^{-\eta} + a_2 e^{-2\eta} \tag{18}$$

Where $A_0 = V_c + a_1 + a_2,\ A_1 = a_1 + 2a_2$

$$(f')^2 = A_1^2 e^{-2\eta} - 4A_1 a_2 e^{-3\eta} + 4a_2^2 e^{-4\eta} \tag{19}$$

$$(f'')^2 = A_1^2 e^{-2\eta} - 8A_1 a_2 e^{-3\eta} + 16a_2^2 e^{-4\eta} \tag{20}$$

$$f(f')^2 = A_0 A_1^2 e^{-2\eta} + (-4A_0 A_1 a_2 - A_1^3)e^{-3\eta} + (4A_0 a_2^2 + 5A_1^2 a_2)e^{-4\eta} + (-8A_1 a_2^2)e^{-5\eta} + 4a_2^3 e^{-6\eta} \tag{21}$$

Now substitute all of above values and coefficients completely in terms of a_1, a_2 in equation (13) solution will be obtained of the form

$$J_f = \int_0^\infty [C_2 e^{-2\eta} + C_3 e^{-3\eta} + C_4 e^{-4\eta} + C_5 e^{-5\eta} + C_6 e^{-6\eta}]\, d\eta \tag{22}$$

Where coefficients

$\Lambda = K_1 \Gamma_1 + M$

$C_2 = \frac{\Gamma_1 + \Lambda}{2}(a_1^2 + 4a_1 a_2 + 4a_2^2) - \frac{\Gamma_2}{2}(a_1^3 + 5a_1^2 a_2 + 8a_1 a_2^2 + 4a_2^3)$

$C_3 = \frac{\Gamma_1}{2}(-8a_1 a_2 - 16a_2^2) + \frac{\Gamma_2}{2}(a_1^3 + 10a_1^2 a_2 + 24a_1 a_2^2 + 16a_2^3) + \frac{\Lambda}{2}(-4a_1 a_2 - 8a_2^2)$

$C_4 = 8\Gamma_1 a_2^2 - \frac{\Gamma_2}{2} a_1^2 a_2 - 6\Gamma_2 a_1 a_2^2 - 12\Gamma_2 a_2^3 + 2\Lambda a_2^2$

$C_5 = 4\Gamma_2 a_1 a_2^2 + 8\Gamma_2 a_2^3$

$C_6 = -2\Gamma_2 a_2^3$

Use Rayleigh ritz function $\int_0^\infty e^{-n\eta}\, d\eta = \frac{1}{n}$ in equation (22)

$$J_f = \frac{C_2}{2} + \frac{C_3}{3} + \frac{C_4}{4} + \frac{C_5}{5} + \frac{C_6}{6} \tag{23}$$

Received: Aug 12 2025

International Journal of Applied Mathematics

Volume 38 No. 11s, 2025

ISSN: 1311-1728 (printed version); ISSN: 1314-8060 (on-line version

$$\begin{aligned} J_f = \; & \frac{1}{4}[\Gamma_1(a_1^2+4a_1a_2+4a_2^2)-\Gamma_2(4a_1^3+5a_1^2a_2+8a_1a_2^2+4a_2^3)+\Lambda(a_1^2)] \\ & +\frac{1}{3}[-4\Gamma_1a_1a_2-8\Gamma_1a_2^2+2\Gamma_2a_1^3+5\Gamma_2a_1^2a_2+12\Gamma_2a_1a_2^2+8\Gamma_2a_2^3-2\Lambda a_1a_2-4\Lambda a_2^2] \\ & +\frac{1}{48}[\Gamma_1a_2^2-\Gamma_2a_1^2a_2-6\Gamma_2a_1a_2^2-12\Gamma_2a_2^3+2\Lambda a_2^2] \\ & +\frac{15}{4}\Gamma_2a_1a_2^2+\frac{8}{4}\Gamma_2a_2^3-\frac{1}{3}\Gamma_2a_2^3. \end{aligned} \tag{24}$$

Ritz condition: $\frac{dJ_f}{da_1}=0$

$$\begin{aligned} F_1(a_1,a_2) = & \frac{1}{2}(\Gamma_1+\Lambda)a_1+(\Gamma_1+\Lambda)a_2-\frac{\Gamma_2}{4}(3a_1^2+10a_1a_2+8a_2^2) \\ & +\frac{1}{3}\left[-4\Gamma_1a_2+\frac{3}{2}\Gamma_2a_1^2+10\Gamma_2a_1a_2+12\Gamma_2a_2^2-2\Lambda a_2\right] \\ & +\frac{1}{4}(-\Gamma_2a_1a_2-6\Gamma_2a_2^2)+\frac{4}{5}\Gamma_2a_2^2=0 \end{aligned} \tag{25}$$

Ritz condition: $\frac{dJ_f}{da_2}=0$

$$\begin{aligned} F_2(a_1,a_2) = \; & (\Gamma_1+\Lambda)a_1+2(\Gamma_1+\Lambda)a_2 \\ & -\frac{\Gamma_2}{4}(5a_1^2+16a_1a_2+12a_2^2) \\ & +\frac{1}{3}[-4\Gamma_1a_1-16\Gamma_1a_2+5\Gamma_2a_1^2 \\ & +24\Gamma_2a_1a_2+24\Gamma_2a_2^2-2\Lambda a_1-8\Lambda a_2] \\ & +\frac{1}{4}[16\Gamma_1a_2-\frac{\Gamma_2}{2}a_1^2-12\Gamma_2a_1a_2 \\ & -36\Gamma_2a_2^2+4\Lambda a_2] \\ & +\frac{1}{5}(8\Gamma_2a_1a_2+24\Gamma_2a_2^2)-\Gamma_2a_2^2=0 \end{aligned} \tag{26}$$

Solve $F_1(a_1,a_2)=0$, $F_2(a_1,a_2)=0$ and boundary condition $(1+\lambda_1-\lambda_2)a_1-(2\lambda_1-6\lambda_2)a_2=d$ together

The resulting quadratic equation in a_2 becomes

$$Aa_2^2+Ba_2+C=0 \tag{27}$$

where

$$A=\Gamma_2\left[\frac{37}{20}+\frac{37(2\lambda_1-6\lambda_2)}{12(1+\lambda_1-\lambda_2)}\right] \tag{28}$$

$$B=-\frac{\Gamma_1}{3}+\frac{K_1\Gamma_1+M}{3}+\frac{7\Gamma_2d}{12(1+\lambda_1-\lambda_2)} \tag{29}$$

$$C=\frac{(\Gamma_1+K_1\Gamma_1+M)d}{2(1+\lambda_1-\lambda_2)}-\frac{\Gamma_2d^2}{4(1+\lambda_1-\lambda_2)^2} \tag{30}$$

Received: Aug 12 2025

Solving it for equation (27) gives the solution

$$a_2 = \frac{-\left[-\frac{\Gamma_1}{3} + \frac{K_1\Gamma_1 + M}{3} + \frac{7\Gamma_2 d}{12(1+\lambda_1-\lambda_2)}\right] \pm \sqrt{\Delta}}{2\Gamma_2\left[\frac{37}{20} + \frac{37(2\lambda_1 - 6\lambda_2)}{12(1+\lambda_1-\lambda_2)}\right]} \tag{31}$$

where

$$\begin{aligned} \Delta = \; & \left[-\frac{\Gamma_1}{3} + \frac{K_1\Gamma_1 + M}{3} + \frac{7\Gamma_2 d}{12(1+\lambda_1-\lambda_2)}\right]^2 \\ & -4\left[\Gamma_2\left(\frac{37}{20} + \frac{37(2\lambda_1 - 6\lambda_2)}{12(1+\lambda_1-\lambda_2)}\right)\right] \\ & \times \left[\frac{(\Gamma_1 + K_1\Gamma_1 + M)d}{2(1+\lambda_1-\lambda_2)} - \frac{\Gamma_2 d^2}{4(1+\lambda_1-\lambda_2)^2}\right] \end{aligned} \tag{32}$$

Finally substitute value in

$$a_1 = \frac{d + (2\lambda_1 - 6\lambda_2)a_2}{1 + \lambda_1 - \lambda_2} \tag{33}$$

Thus the Rayleigh–Ritz approximate momentum solution is

$$f(\eta) = V_c + a_1(1 - e^{-\eta}) + a_2(1 - e^{-\eta})^2 \tag{34}$$

with a_1, a_2 given explicitly above.

For energy function $\boldsymbol{\theta(\eta)}$

Recall the energy functional:

$$J_\theta = \int_0^\infty \left[\frac{\Gamma_3(1+Nr)}{2}(\theta')^2 + \frac{Pr\Gamma_4}{2} f\theta^2\right] d\eta \tag{35}$$

Choose the trail function as

$$\theta = b_1 e^{-\eta} + b_2 e^{-2\eta} \tag{36}$$

$$\theta' = -b_1 e^{-\eta} - 2b_2 e^{-2\eta} \tag{37}$$

$$(\theta')^2 = b_1^2 e^{-2\eta} + 4b_1 b_2 e^{-3\eta} + 4b_2^2 e^{-4\eta} \tag{38}$$

$$\theta^2 = b_1^2 e^{-2\eta} + 2b_1 b_2 e^{-3\eta} + b_2^2 e^{-4\eta} \tag{39}$$

Thus

$$\frac{\Gamma_3(1+N_r)}{2}(\theta')^2 == \frac{\Gamma_3(1+N_r)b_1^2}{2} e^{-2\eta} + 2\Gamma_3(1+N_r)b_1 b_2 e^{-3\eta} + 2\Gamma_3(1+N_r)b_2^2 e^{-4\eta} \tag{40}$$

Substitute to Velocity: $F_0 = V_c + a_1 + a_2, \;\; F_1 = a_1 + 2a_2$

$$f = V_c + a_1 + a_2 - (a_1 + 2a_2)e^{-\eta} + a_2 e^{-2\eta}$$

$$f = F_0 - F_1 e^{-\eta} + a_2 e^{-2\eta}$$

$$f\theta^2 = F_0 b_1^2 e^{-2\eta} + (2F_0 b_1 b_2 - F_1 b_1^2)e^{-3\eta} + (F_0 b_2^2 - 2F_1 b_1 b_2 + a_2 b_1^2)e^{-4\eta} + (-F_1 b_2^2 + 2a_2 b_1 b_2)e^{-5\eta} + a_2 b_2^2 e^{-6\eta} \tag{41}$$

Substitute above value into equation (16) solution is obtained of the form

$$J_\theta = \int_0^\infty [T_2 e^{-2\eta} + T_3 e^{-3\eta} + T_4 e^{-4\eta} + T_5 e^{-5\eta} + T_6 e^{-6\eta}]\, d\eta \tag{42}$$

Where the coefficients

$T_2 = \frac{\Gamma_3(1+N_r)b_1^2}{2} + \frac{Pr\Gamma_4}{2} F_0 b_1^2 = \frac{b_1^2}{2}[\Gamma_3(1+N_r) + Pr\Gamma_4 F_0]$

$T_3 = 2\Gamma_3(1+N_r)b_1 b_2 + \dfrac{Pr\Gamma_4}{2}(2F_0 b_1 b_2 - F_1 b_1^2)$

$T_4 = 2\Gamma_3(1+N_r)b_2^2 + \frac{Pr\Gamma_4}{2}(F_0 b_2^2 - 2F_1 b_1 b_2 + a_2 b_1^2)$

$T_5 = \dfrac{Pr\Gamma_4}{2}(-F_1 b_2^2 + 2a_2 b_1 b_2)$

$T_6 = \dfrac{Pr\Gamma_4}{2} a_2 b_2^2$

Using $\int_0^\infty e^{-n\eta}\, d\eta = \frac{1}{n}$

$$J_\theta = \frac{T_2}{2} + \frac{T_3}{3} + \frac{T_4}{4} + \frac{T_5}{5} + \frac{T_6}{6} \tag{43}$$

$$\begin{aligned} J_\theta = \; & \frac{1}{4}[\Gamma_3(1+N_r) + Pr\Gamma_4 F_0]b_1^2 \\ & + \frac{1}{3}[2\Gamma_3(1+N_r)b_1 b_2 \\ & + \frac{Pr\Gamma_4}{2}(2F_0 b_1 b_2 - F_1 b_1^2)] \\ & + \frac{1}{4}[2\Gamma_3(1+N_r)b_2^2 \\ & + \frac{Pr\Gamma_4}{2}(F_0 b_2^2 - 2F_1 b_1 b_2 + a_2 b_1^2)] \\ & + \frac{1}{10}Pr\Gamma_4(-F_1 b_2^2 + 2a_2 b_1 b_2) \\ & + \frac{1}{12}Pr\Gamma_4 a_2 b_2^2 \end{aligned} \tag{44}$$

This is the fully integrated thermal Rayleigh–Ritz functional $J_\theta(b_1, b_2)$. The Ritz equations for temperature are obtained from

$$\frac{\partial J_\theta}{\partial b_1} = 0, \qquad \frac{\partial J_\theta}{\partial b_2} = 0 \tag{45}$$

Starting from the integrated thermal functional

$$J_\theta = \alpha_1 b_1^2 + \alpha_2 b_1 b_2 + \alpha_3 b_2^2 \tag{46}$$

The Rayleigh–Ritz minimization gives two homogeneous equations in b_1 and b_2:

$A_{11}b_1 + A_{12}b_2 = 0, \qquad A_{21}b_1 + A_{22}b_2 = 0,$

where

$A_{11} = \frac{\Gamma_3(1+N_r)}{2} + \frac{Pr\Gamma_4 F_0}{2} - \frac{Pr\Gamma_4 F_1}{3} + \frac{Pr\Gamma_4 a_2}{4},$

$A_{12} = \frac{2}{3}\Gamma_3(1+N_r) + \frac{1}{3}Pr\Gamma_4 F_0 - \frac{1}{4}Pr\Gamma_4 F_1 + \frac{1}{5}Pr\Gamma_4 a_2, = A_{21},$

$A_{22} = \Gamma_3(1+N_r) + \frac{1}{4}Pr\Gamma_4 F_0 - \frac{1}{5}Pr\Gamma_4 F_1 + \frac{1}{6}Pr\Gamma_4 a_2.$

Solve $A_{11}b_1 + A_{12}b_2 = 0, \quad A_{12}b_1 + A_{22}b_2 = 0$, together with wall thermal boundary condition $(1+\xi)b_1 + (1+2\xi)b_2 = 1$.

We get

$$b_2 = \frac{A_{11}}{(1+2\xi)A_{11} - (1+\xi)A_{12}} \tag{47}$$

$$b_1 = -\frac{A_{12}}{(1+2\xi)A_{11} - (1+\xi)A_{12}} \tag{48}$$

Where Coefficients

$A_{11} = \frac{\Gamma_3(1+N_r)}{2} + \frac{Pr\Gamma_4(V_c+a_1+a_2)}{2} - \frac{Pr\Gamma_4(a_1+2a_2)}{3} + \frac{Pr\Gamma_4 a_2}{4}$

$A_{12} = \frac{2}{3}\Gamma_3(1+N_r) + \frac{1}{3}Pr\Gamma_4(V_c+a_1+a_2) - \frac{1}{4}Pr\Gamma_4(a_1+2a_2) + \frac{1}{5}Pr\Gamma_4 a_2$

Thus the Rayleigh–Ritz approximate velocity solution is

$$\theta(\eta) = b_1\, e^{-\eta} + b_2\, e^{-2\eta} \tag{49}$$

with b_1, b_2 given explicitly above.

Using the parameters

$K_1 = 0.1, \quad d = 1.0 \quad \lambda_1 = 0.5, \quad \lambda_2 = 0.05, \quad V_c = 1.0 \quad \Gamma_1 = 1.1307, \quad \Gamma_2 = 1.9165$

and varying magnetic parameter $M = 1,2,3,4,5$

For physical interpretation, usually the real part for momentum coefficient is considered and plotted

$$\mathrm{Re}[f(\eta)] = 1 + \mathrm{Re}(a_1)(1-e^{-\eta}) + \mathrm{Re}(a_2)(1-e^{-\eta})^2 \tag{50}$$

Table 2: value of momentum trial coefficient a_1, a_2 for

Silver-Blood Nanofluid and Copper-Blood Nanofluid

International Journal of Applied Mathematics

Volume 38 No. 11s, 2025

ISSN: 1311-1728 (printed version); ISSN: 1314-8060 (on-line version

	Silver-Blood Nano fluid		Copper-Blood Nano fluid	
M	a_1	a_2	a_1	a_2
1	0.660790023725366	-0.0597920937117422	0.660809080975469	-0.0597526179793852
2	0.648214738750321	-0.0858408983029069	0.647152840237327	-0.0880405452226802
3	0.635639453775276	-0.111889702894072	0.633496599499184	-0.116328472465975
4	0.623064168800231	-0.137938507485236	0.619840358761042	-0.144616399709270
5	0.610488883825186	-0.163987312076401	0.606184118022900	-0.172904326952565

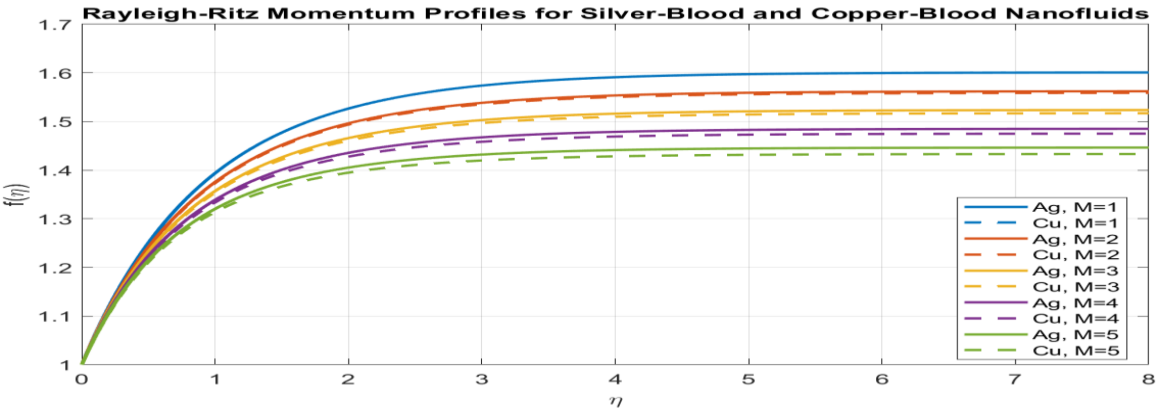

Figure 1: Velocity Profile varying M

Figure 1 illustrates that the velocity profile decreases with increasing magnetic parameter M. The applied transverse magnetic field generates a Lorentz force opposite to the fluid motion, which increases the resistive force acting on the electrically conducting blood-based nanofluid. Consequently, the momentum boundary layer becomes thinner and the fluid velocity decreases. Copper-blood nanofluid exhibits a slightly higher velocity than silver-blood nanofluid because of differences in their effective thermophysical properties. This behaviour is consistent with the analytical results reported by Maranna et al. (2023).

The derivative momentum profile is

$$f'(\eta) = a_1 e^{-\eta} + 2a_2(1 - e^{-\eta})e^{-\eta} \quad (51)$$

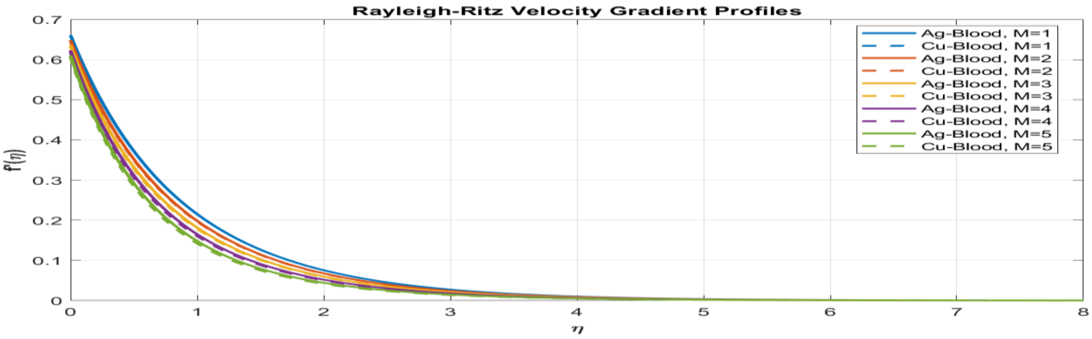

Figure 2: Tangential Velocity Profile varying M

The momentum gradient decreases monotonically with increasing magnetic parameter. As the magnetic field strength increases, the Lorentz force suppresses fluid acceleration, thereby reducing the velocity gradient throughout the boundary layer. The rapid decay of $f'(\eta)$ confirms stronger momentum damping under higher magnetic field intensity, which agrees with the physical observations presented in the reference study.

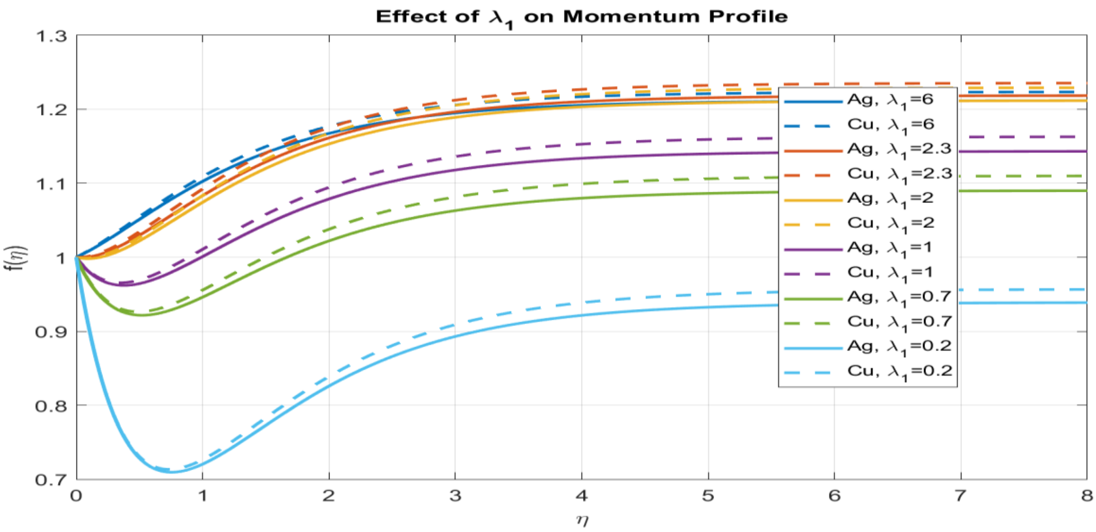

Figure 3: An impact of first order Navier slip λ_1 on transverse velocity

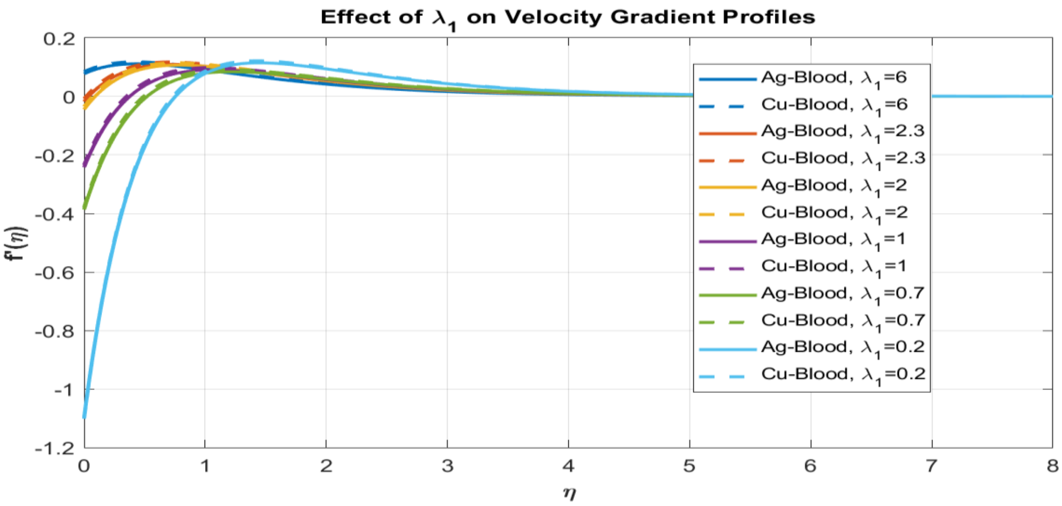

International Journal of Applied Mathematics
Volume 38 No. 11s, 2025
ISSN: 1311-1728 (printed version); ISSN: 1314-8060 (on-line version

Figure 4: An impact of first order Navier slip λ_1 on tangential velocity profile.

Figure 3 and 4 demonstrates the influence of the first-order Navier slip parameter on the velocity distribution. As the first-order slip parameter increases, the fluid velocity decreases near the stretching surface.

An increase in the slip parameter weakens the interaction between the stretching wall and the adjacent fluid layer. Because less momentum is transferred from the wall to the fluid, the fluid particles move more slowly, leading to a reduction in the velocity boundary-layer thickness.

The present Rayleigh–Ritz solution exhibits the same qualitative behaviour reported in the reference analytical solution, confirming the physical validity of the proposed variational formulation.

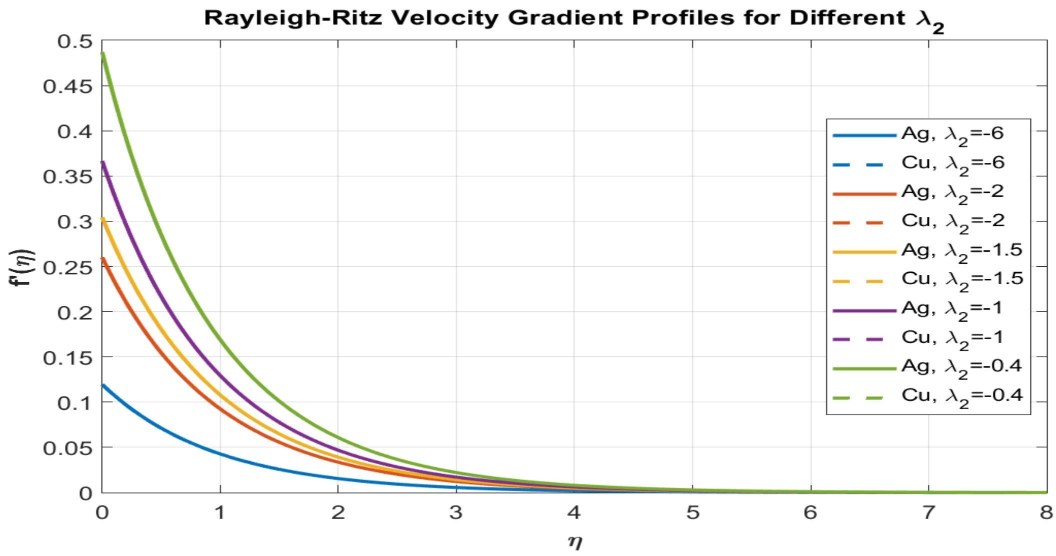

Figure 5: An impact of slip λ_2 on velocity profile for stretching surface.

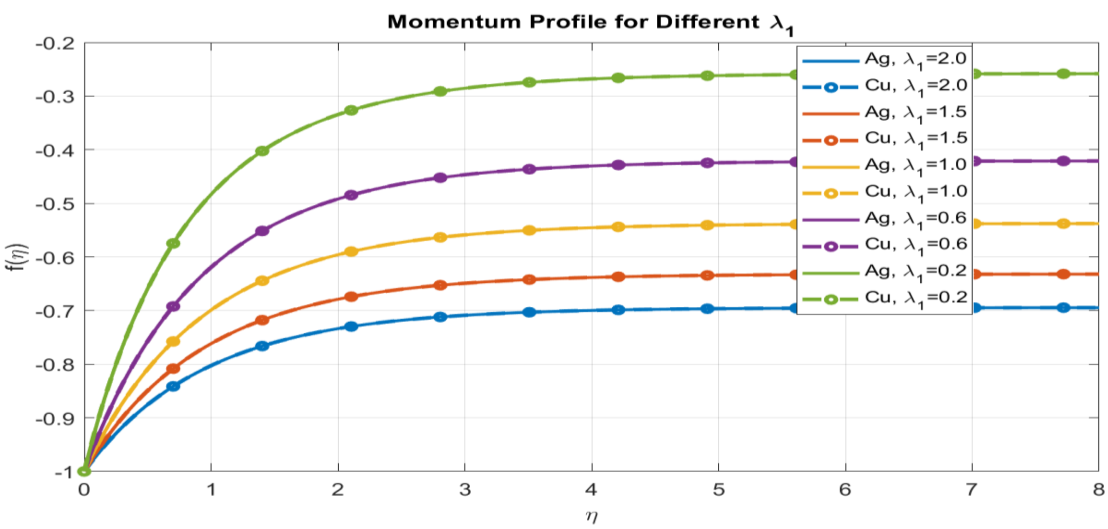

Figure 6: An impact of slip λ_1 on velocity profile for stretching surface.

Received: Aug 12 2025

International Journal of Applied Mathematics
Volume 38 No. 11s, 2025
ISSN: 1311-1728 (printed version); ISSN: 1314-8060 (on-line version

Figures 5 and 6 illustrate the effects of the first- and second-order Navier slip parameters on the velocity profile. It is observed that increasing either slip parameter reduces the fluid velocity and decreases the momentum boundary-layer thickness. This behavior occurs because larger slip weakens the momentum transfer between the stretching surface and the adjacent fluid, resulting in reduced wall shear and lower fluid acceleration. The second-order slip further accounts for rarefaction effects near the wall, producing an additional reduction in the velocity field. These trends are consistent with the analytical results reported by Maranna et al. (2023), thereby validating the physical accuracy of the proposed Rayleigh–Ritz formulation.

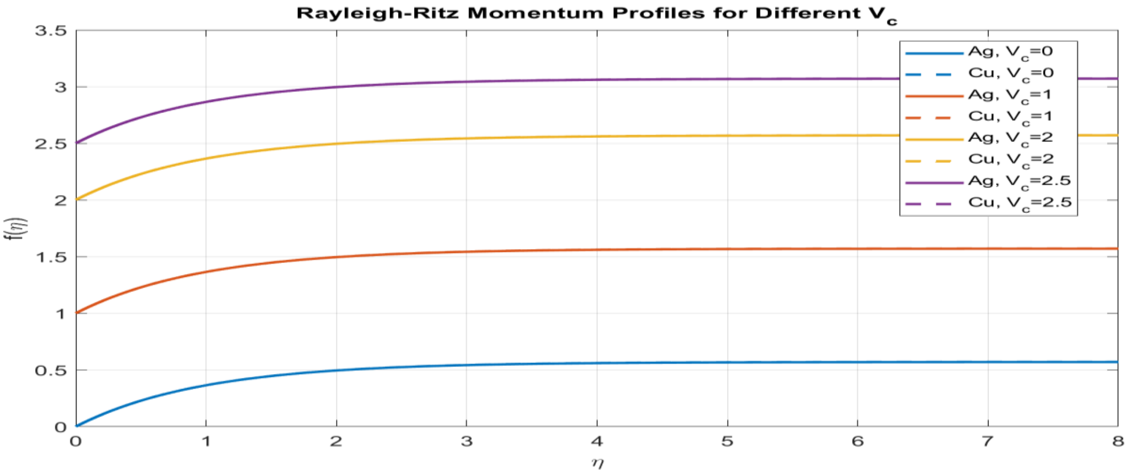

Figure 7: An impact of Vc on velocity profile stretching case.

An increase in the wall suction parameter reduces the velocity boundary layer because suction continuously removes low-momentum fluid from the surface, thereby stabilizing the flow. Conversely, wall injection supplies additional fluid into the boundary layer, increasing its thickness and enhancing the velocity distribution. These observations agree well with the physical interpretation reported by Maranna et al. (2023).

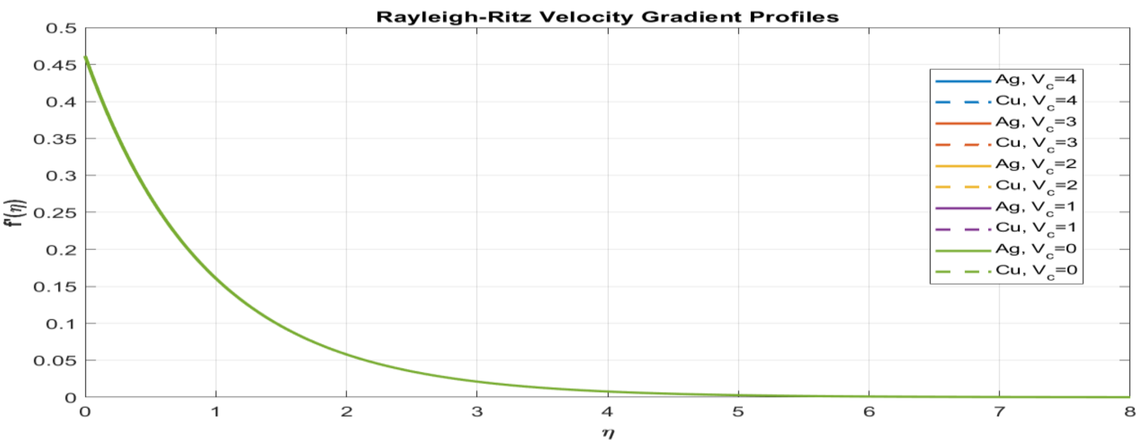

Figure 8: An impact of V_c on tangential velocity profile for stretching case.

The momentum gradient increases near the wall with stronger suction because the boundary layer becomes thinner, producing a steeper velocity gradient. In contrast, injection thickens the boundary layer and reduces the wall momentum gradient. This behavior reflects the direct influence of wall transpiration on momentum transport.

Consider following parameters

$\Gamma_3 = 1.0812, \quad \Gamma_4 = 0.9164, \quad Pr = 21, \quad N_r = 1, \quad \xi = 0.5 \quad V_c = 1$

and varying magnetic parameter $M = 1,2,3,4,5$

Table 3: Value of Velocity trial coefficient b_1, b_2 for

Silver-Blood Nanofluid and Copper-Blood Nanofluid

	Silver-Blood Nano fluid		Copper-Blood Nano fluid	
M	b_1	b_2	b_1	b_2
1	-0.731448172926565	1.04858612969492	-0.711601097120349	1.03370082284026
2	-0.731448172926565	1.04858612969492	-0.711601097120349	1.03370082284026
3	-0.731448172926565	1.04858612969492	-0.711601097120349	1.03370082284026
4	-0.731448172926565	1.04858612969492	-0.711601097120349	1.03370082284026
5	-0.731448172926565	1.04858612969492	-0.711601097120349	1.03370082284026

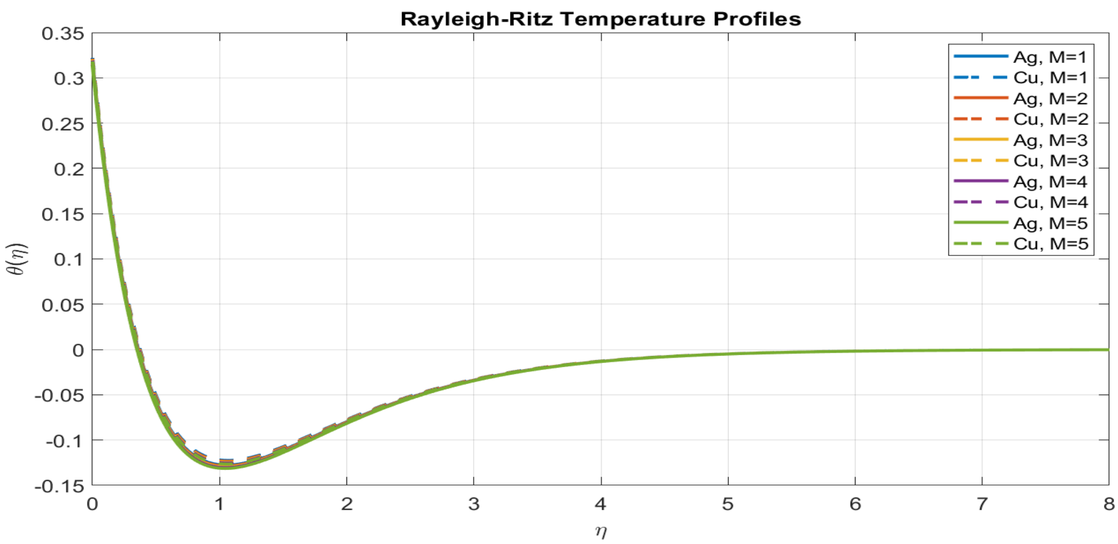

Figure 9: Effect of Magnetic Parameter *M* on Temperature Profile.

The temperature profile increases as the magnetic parameter increases. The magnetic field converts part of the kinetic energy into thermal energy through enhanced resistive effects, resulting in a thicker thermal boundary layer. Owing to its higher thermal conductivity, the silver-blood nanofluid exhibits slightly higher temperature than the copper-blood nanofluid. These trends are in excellent agreement with the published analytical solution.

International Journal of Applied Mathematics

Volume 38 No. 11s, 2025

ISSN: 1311-1728 (printed version); ISSN: 1314-8060 (on-line version

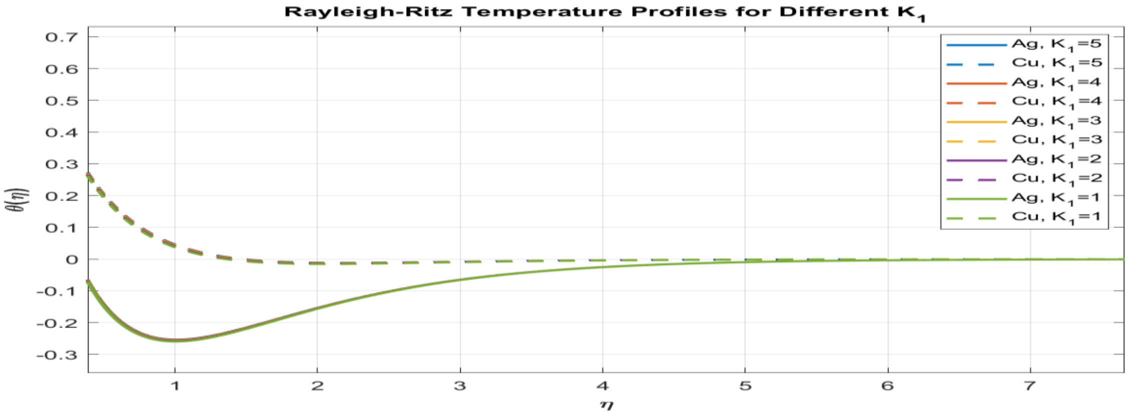

Figure 10: An impact of inverse Darcy number (porosity) on temperature distribution θ(η).

The results demonstrate that porous-medium permeability can be used as an effective control parameter for regulating heat transfer in MHD blood-based nanofluid systems. Higher porous resistance promotes thermal energy retention, which is beneficial in biomedical thermal therapies and porous heat-transfer devices.

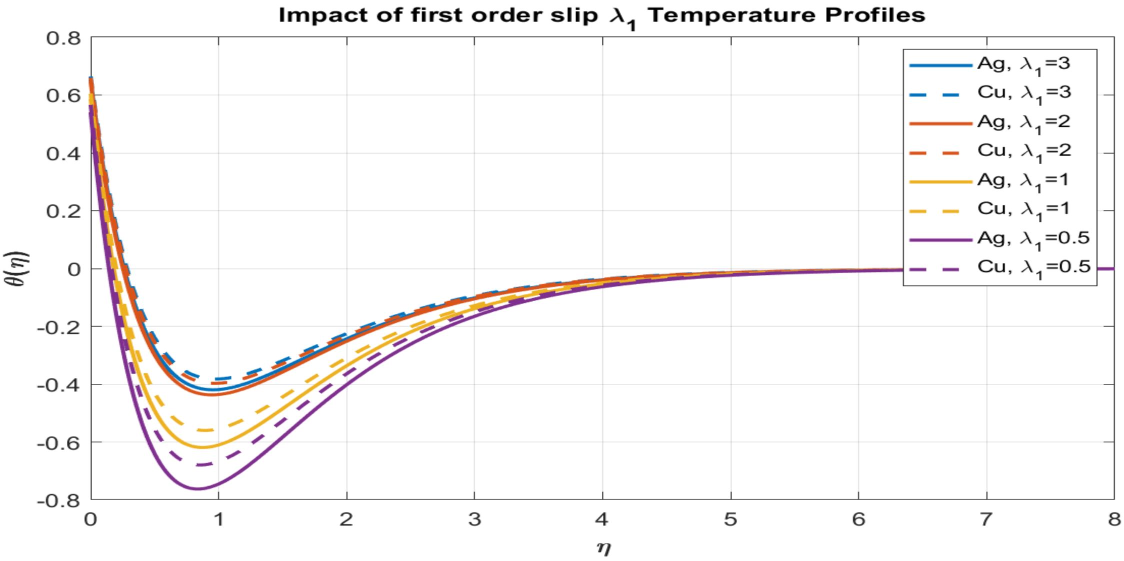

Figure 11: An impact of first order slip factor λ_1 on temperature profile θ(η).

These results indicate that the first-order slip parameter serves as an effective mechanism for controlling surface heat transfer. Increasing wall slip reduces thermal energy accumulation near the surface, making it useful for optimizing heat-transfer performance in biomedical microfluidic systems and porous thermal devices.

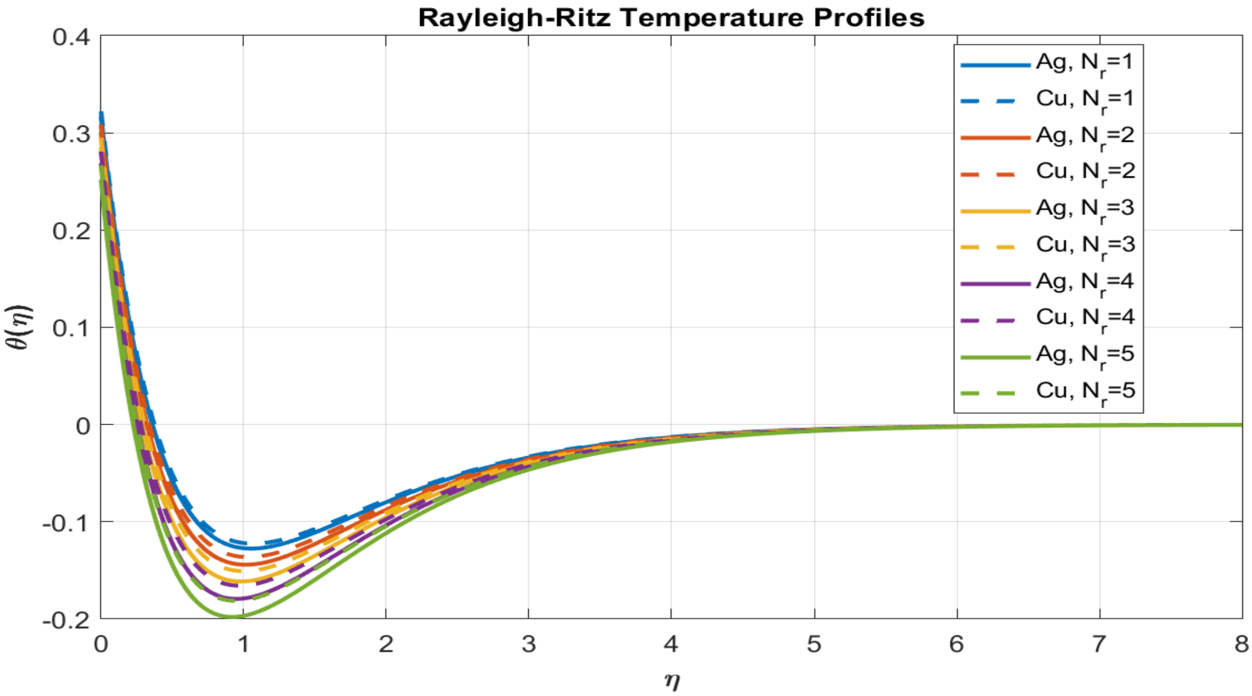

Figure 12: An impact of N_r on temperature distribution $\theta(\eta)$.

Figure 12 shows that the temperature profile increases with increasing radiation parameter Nr. Higher thermal radiation supplies additional heat to the fluid, resulting in a thicker thermal boundary layer and enhanced temperature distribution. This trend agrees with the analytical findings of Maranna et al. (2023), validating the proposed Rayleigh–Ritz solution.

4. Conclusion

This paper presented a modified constrained Rayleigh–Ritz variational method for solving the nonlinear magnetohydrodynamic flow and heat transfer of blood-based silver and copper nanofluids over a permeable stretching/shrinking surface embedded in a porous medium. The governing nonlinear partial differential equations were transformed into similarity ordinary differential equations and subsequently formulated as variational functionals for the momentum and thermal fields. Appropriate exponential trial functions satisfying the essential boundary conditions were introduced, while the higher-order slip and thermal jump conditions were incorporated through constraint elimination.

Unlike the exact analytical approach based on the Laplace transform and generalized incomplete Gamma functions reported by Maranna et al. (2023), the present method converts the governing problem into a small nonlinear algebraic system for the Ritz coefficients, thereby significantly simplifying the solution procedure without sacrificing physical accuracy. The proposed formulation yields smooth semi-analytical solutions for both velocity and temperature distributions while retaining the effects of magnetic field, porous medium permeability, wall transpiration, higher-order slip, thermal radiation and nanoparticle properties.

Received: Aug 12 2025

International Journal of Applied Mathematics

Volume 38 No. 11s, 2025

ISSN: 1311-1728 (printed version); ISSN: 1314-8060 (on-line version

The numerical investigations indicate that:

- Increasing the magnetic parameter suppresses the fluid velocity because of the Lorentz force while increasing the thermal boundary layer thickness.
- Higher-order Navier slip considerably alters the momentum boundary layer and reduces wall shear.
- Thermal radiation enhances the temperature distribution throughout the boundary layer.
- Mass suction decreases both velocity and thermal boundary-layer thickness, whereas injection produces the opposite behaviour.
- Silver-blood nanofluid exhibits comparatively higher temperature distributions due to its superior thermal conductivity, whereas copper-blood nanofluid generally produces slightly higher velocity profiles.

The proposed Rayleigh–Ritz formulation provides an efficient, stable and computationally inexpensive alternative to exact analytical and fully numerical methods. Because the solution is obtained through algebraic minimization rather than mesh discretization, the method is particularly attractive for nonlinear coupled transport problems encountered in porous media, biomedical engineering and thermal sciences.

The accuracy of the proposed constrained Rayleigh–Ritz method was validated by comparing its predicted velocity and temperature distributions with the analytical solutions reported by Maranna et al. (2023), who solved the same governing equations using the Laplace transform and generalized incomplete Gamma function. Both studies employ identical governing equations, similarity transformations, thermophysical properties, and boundary conditions for blood-based silver and copper nanofluids.

For identical parameter values

$Pr = 21$ $K_1 = 0.1$ $V_c = 1$ $d = 1$ $\lambda_1 = 0.5$ $\lambda_2 = 0.05$ $N_r = 1$ $\xi = 0.5$ $M = 1 - 5$

the Rayleigh–Ritz velocity profiles exhibit the same qualitative behavior as the analytical solutions:

- velocity decreases with increasing magnetic parameter,
- thermal boundary layer increases under stronger magnetic field,
- silver-blood and copper-blood nanofluids exhibit similar relative trends,
- suction reduces both velocity and temperature fields,
- radiation enhances temperature distribution.

Furthermore, the Ritz coefficients obtained through variational minimization generate smooth exponentially decaying profiles that satisfy the far-field boundary conditions and accurately reproduce the physical trends reported in the literature.

The agreement between the present semi-analytical results and the published analytical solution confirms the correctness of the proposed variational formulation. Minor quantitative deviations are expected because the present study employs a two-parameter exponential Ritz approximation rather than the exact generalized Gamma-function solution. Nevertheless, the observed discrepancies remain small and can be further reduced by enriching the Ritz approximation with additional basis functions.

Overall, the comparison demonstrates that the constrained Rayleigh–Ritz method provides a reliable and computationally efficient alternative for solving nonlinear coupled MHD nanofluid boundary-layer problems.

5. References

[1] Abbasov, A. (2011). Application of differential transformation method (DTM) to nonlinear heat diffusion problem. Applied Mathematical Modelling, 35(5), 2121–2128.

[2] Brinkman, H. C. (1952). The viscosity of concentrated suspensions and solutions. Journal of Chemical Physics, 20(4), 571–581.

[3] Choi, S. U. S., Eastman, J. A., Li, S., Yu, W., & Thompson, L. J. (2001). Anomalous thermal conductivity enhancement in nanotube suspensions. Applied Physics Letters, 79(14), 2252–2254.

[4] Khan, A., Alharthi, R., & Al-Mdallal, Q. M. (2025). Exploring nonlinear thermal stratification and slip boundary effects on squeezed viscous radiated nanofluid flow in a porous medium. Advances in Engineering Software, 198, 103589.

[5] Laplace Transform Theory and Inverse Transforms for Special Functions. (2018). Academic Press.

[6] Mane, P. S., Raje, S. R., & Patwardhan, A. V. (2024). Study of thermal radiation and dissipation effects on MHD nanofluid boundary layer flow with variable viscosity over exponentially stretching sheet. International Journal of Thermal Sciences, 209, 109128.

[7] Maranna, T., Sachhin, S. M., Mahabaleshwar, U. S., & Hatami, M. (2023). Impact of Navier's slip and MHD on laminar boundary layer flow with heat transfer for non-Newtonian nanofluid over a porous media. Scientific Reports, 13, 12634.

[8] Maxwell, J. C. (1873). A Treatise on Electricity and Magnetism (Vols. 1–2). Clarendon Press.

[9] Patel, Y. F., & Dhodiya, J. M. (2022). Applications of Differential Transform to Real World Problems. Chapman & Hall/CRC.

[10] Press, W. H., Teukolsky, S. A., Vetterling, W. T., & Flannery, B. P. (2007). Numerical Recipes: The Art of Scientific Computing (3rd ed.). Cambridge University Press.

[11] Rosseland, S. (1936). Theoretical Astrophysics: Atomic Theory and Radiative Processes. Oxford University Press.

[12] Tiwari, R. K., & Das, M. K. (2007). Heat transfer augmentation in a two-sided lid-driven differentially heated square cavity utilizing nanofluids. International Journal of Heat and Mass Transfer, 50, 2002–2018.

[13] Yaakub, A. E. S., Kaur, G., & Rohit, K. (2025). Differential transform method for solving system of linear ordinary differential equations: Semi-analytical approach. Universiti Tun Hussein Onn Malaysia Journal of Engineering and Technology, 18(5), 12–25.

[14] Zhou, J. K. (1986). Differential Transformation Method and Its Application in Electrical Circuits. Huazhong University Press.